Soil & Tillage Research 168 (2017) 176–186

Contents lists available at ScienceDirect

Soil & Tillage Research

journal homepage: www.elsevier.com/locate/still

Soil macropore characteristics following conversion of native desert soils to irrigated croplands in a desert-oasis ecotone, Northwest China

Yongyong Zhang[a,*], Wenzhi Zhao[a], Li Fu[b]

[a] Linze Inland River Basin Research Station, Key Laboratory of Eco-hydrology of Inland River Basin, Northwest Institute of Eco-Environment and Resources, Chinese Academy of Sciences, Lanzhou 730000, China
[b] College of Geography and Environment Science, Northwest Normal University, Lanzhou 730070, China

ARTICLE INFO

Article history:
Received 16 July 2016
Received in revised form 18 December 2016
Accepted 8 January 2017
Available online 15 January 2017

Keywords:
Computed tomography
Cultivation
Desert-oasis region
Desert soils
Soil macropores

ABSTRACT

Sustainable use of cultivated desert soils is important for agricultural productivity in desert-oasis ecosystems. However, how soil macropore characteristics may change as a result of agricultural exploitation remains unclear. The objective of this study was to quantify and compare soil properties and macropore characteristics in an old oasis field (>50 years of cultivation, OOF), young oasis field (20 years, YOF), and adjacent uncultivated sandy land (0 year, USL) in Northwest China. Three replicated soil samples were collected from each site to investigate soil properties. Meanwhile, twelve (four replicates by three sites) intact soil core columns, 15 cm in diameter and 30 cm in height, were taken to analyze soil structure. Each soil column was scanned with a helical medical X-ray computed tomography (CT) at a voxel resolution of 0.469 mm × 0.469 mm × 0.600 mm. The results indicated that soil properties and macropore features improved after cultivation. Silt and clay content and dry mean weight diameter (DMWD) of aggregates increased with cultivation time, whereas bulk density decreased. Soil organic carbon and total nitrogen were 7.3 times and 6.7 times greater in soils at the OOF site than USL site, respectively. The increase in silt and clay content and aggregates formation likely resulted from irrigation with silt-laden river water, which in turn impacted soil nutrient accumulation. Soils at the OOF and YOF sites had greater macroporosity compared with soil at USL, and macroporosity also increased with cultivation time. X-ray CT revealed that soil macroporosity was 8.7–18.9 times greater in irrigated croplands than native desert. Soil macropores were mainly distributed at soil depths of 0–200 mm at the OOF and YOF sites, while smaller and less continuous macropores were randomly distributed across soil depths at the USL site. The larger number of macropores at the cultivated sites can be attributed to greater soil organic carbon, tillage-induced soil horizons, and alternate wetting and drying processes. Few soil macropores at the USL site may be associated with wind erosion and soil fauna burrows. Conversion of native desert soils to irrigated croplands had a positive effect on soil pore development in the desert-oasis ecotone.

1. Introduction

The history of agricultural exploitation in the Hexi Corridor of Gansu Province has been one of land conversion from virgin desert to arable soils. This continuous process of expansion of cultivated oases has intensified as the human population has increased. The expansion of oases has significantly increased the area of arable land as well as grain production, and it has altered landscape patterns in this arid region (Huang et al., 2007; Li et al., 2009a, 2009b; Su et al., 2010). Nonetheless, Environmental risks to agriculture such as water shortage, drought, and wind erosion remain serious. Owing to the hot, dry climate, the evolution of desert soils can be slow and clay and organic matter contents are often low (Zhao et al., 2006). As a result, these soils have a naturally loose structure, a shortage of aggregates (Li et al., 2006), and are susceptible to wind erosion, especially under conventional tillage. Therefore, sustainable agricultural use of cultivated desert soils has become a concern in desert-oasis regions. However, the effects of cultivation on soil structure, especially on macropore characteristics, remain poorly understood.

Soil macropores are critical to its function as a pathway for water, air, and chemical movement (Luo et al., 2010a, 2010b). Macropores are large soil voids and pathways including earthworm burrows, root channels, fissures and interaggregate voids,

* Corresponding author.
E-mail address: zhangxyz23@126.com (Y. Zhang).

http://dx.doi.org/10.1016/j.still.2017.01.004
0167-1987/

that are often distinct from the soil matrix, and which can permit preferential flow of water and nutrients through the soil profile (Jarvis, 2007; Li et al., 2009a, 2009b; Helliwell et al., 2013). Although macropores constitute only a small percentage of total porosity, they have a critical influence on saturated flow (Luxmoore et al., 1990; Lin et al., 1996). Macropores can cause chemicals and contaminants to be transported into the groundwater (Beven and Germann, 1982; Lin et al., 2005; Jarvis, 2007); nevertheless, they also have many benefits such as better aeration, root development, improved nutrient cycling in a well-developed soil structure (Jarvis et al., 2012). Macropore networks are shaped by factors related to soil structural hierarchy, including the abundance and activity of soil biota such as earthworms, soil properties (e.g. clay content), site factors (e.g. slope position, drying intensity, vegetation cover) and management (e.g. cropping, tillage, traffic) (Jarvis et al., 2012; Jassogne et al., 2007; Kumar et al., 2010; Li et al., 2016). Soil type, land use, and vegetation type are important factors influencing soil pore characteristics (Gantzer and Anderson, 2002; Udawatta et al., 2008; Mooney and Morris, 2008; Hu et al., 2016). For example, soil type, land use, and their interaction have been demonstrated to significantly alter macroporosity, macropore network density, surface area, length density, node density, and mean angle (Luo et al., 2010a). Hu et al. (2015) also reported that shrub encroachment resulting from anthropogenic disturbance significantly influenced soil macropores in grasslands. The alternate flooding and drying in paddy fields produced soil cracks which increased average macropore length but decreased the number of macropores, and changed macropore size distribution and macropore area density distribution with soil depth (Zhang et al., 2015). The process of converting desert to oasis is therefore expected to have a large impact on soil macropore characteristics. Thus visualization and quantification of soil macropore characteristics are essential for better understanding of soil hydrological processes in desert-oasis regions.

The three-dimensional (3-D) structure of soil macropore networks are complex but can be elucidated using X-ray computed tomography (CT) (Turberg et al., 2014; Zhang et al., 2015). A non-invasive imaging technique, CT scanning allows visualization at a much higher resolution than previous methods, such as dye tracing and soil thin sectioning (Grevers et al., 1989; Capowiez et al., 2003; Zhang et al., 2015). Compared with two-dimensional characterizations of soil macropore, such as from photography or manual measurement (Bandyopadhyay et al., 2003; Peng et al., 2006), the 3-D visualization by CT imaging provides greater detail about the shape and complexity of soil macropores. While some methods have been developed to quantity 3-D soil macropore networks (Abou Najm et al., 2010), these assume that the shape of soil macropores are regular, ignoring observed macropore complexity and irregularities (Ringrose-Voase and Sanidad, 1996; Bandyopadhyay et al., 2003). Katuwal et al. (2015) proposed that linking rapid X-ray CT scanning with classical fluid transport measurements on large, intact soil columns was very useful for characterizing soil macropore function. Hu et al. (2016) also quantified 3-D soil macropore networks beneath alpine vegetation using multi-slice helical medical CT. Therefore, quantitative data on soil pore features obtained by CT scanning, especially 3-D macropore networks, are expected to become more readily obtainable and widely available.

The oasis area in the Hexi Corridor has expanded as the desert has been converted to oasis. Previous studies have focused on the effects of land use changes and subsequent management practices on soil properties in this region (Li et al., 2006; Su et al., 2010). However, changes in soil macropore networks as a result of the agricultural exploitation of desert soils remain poorly understood in extremely arid regions. The objective of this study was to quantify the changes in soil properties and macropore features for soils beneath an old oasis field (>50 years of cultivation, OOF), young oasis field (20 years, YOF), and adjacent uncultivated sandy land (as a control, USL) in a desert-oasis region. This study should provide greater understanding of the evolution of soil pore characteristics as the desert is converted to arable land.

2. Materials and methods

2.1. Study site description

The study was conducted in the Linze oasis which is located in the middle reaches of the Heihe River, in the Hexi corridor of Gansu province (100°07′E, 39°24′N, AMSL 1383 m; Fig. 1a). The north of the oasis is the Badain Jaran Desert, covered by sand dunes and gravel Gobi. The study area has an arid climate characterized by cold winters and hot dry summers. The average annual temperature is 7.6 °C; while annual precipitation averages 117 mm and annual hours of sunshine reach 3051.1 h. Annual pan evaporation averages 2388 mm, which is twenty times greater than the annual precipitation. Annual wind speed averages 3.2 m/s. High winds and wind storms often occur in this area (Zhang and Zhao, 2015). Zonal soil is classified as the Calciorthids according to USDA Soil Taxonomy (Zhang, 2001). Owing to long-term wind erosion and deposition of aeolian sands, Psamments tend to form on the margin of the oasis (Su et al., 2010). Peripheral sandy lands have been gradually reclaimed for agricultural use since the 1960s; hence, irrigated croplands in this region range age from 1 year to more than 50 years old. Major landscape types in the study region include the peripheral desert, desert-oasis ecotone, and central oasis.

2.2. Soil sampling and analysis

Personal interviews were held with farm owners in the study area in order to document the history of land use for crop production. Prior to reclamation in the desert-oasis ecotone, the croplands were natural sandy land. The same soil parent materials were found in both the croplands and the adjacent sandy areas (Su et al., 2010). Particle size distributions and organic carbon concentrations in soil horizons were fairly similar at the beginning of croplands in different periods in the study area (Su et al., 2007). How long croplands have been cultivated was determined using the records from the Linze Inland River Basin Research Station, Chinese Academy of Sciences. The station was established in 1975 and is located in the center of the study area.

Two irrigated croplands reclaimed from natural sandy land and one uncultivated sandy land (as the control) were selected for study (Fig. 1b). The three sites were chosen to allow identification of potential changes in soil properties and macropores within different cultivation periods. Monitoring in the uncultivated sandy land was conducted 2–3 km away from the croplands (Fig. 1b). The first irrigated cropland was reclaimed for agricultural use 20 years ago and hence was designated for the purpose of this study, as the “young oasis field” (YOF). The other cropland had been cultivated for crop production for more than 50 years, and was designated the “old oasis field” (OOF). The adjacent “uncultivated sandy land” (0 year, USL) was considered to be the control as it had never been utilized for agriculture. In the YOF and OOF sites, major crops grown include maize (*Zea mays* L.) and spring wheat (*Triticum aestivum* L.), with only one annual harvest. Most cultivation consisted of strip intercropping of spring wheat and maize from 1980 to 2000. In recent years, however, seed maize production has become the pre-dominant agricultural use in these croplands. Monoculture of spring maize mulched with plastic mulching has been grown in the study area for more than ten years. Irrigated croplands were sown with maize on April 10th and harvested on

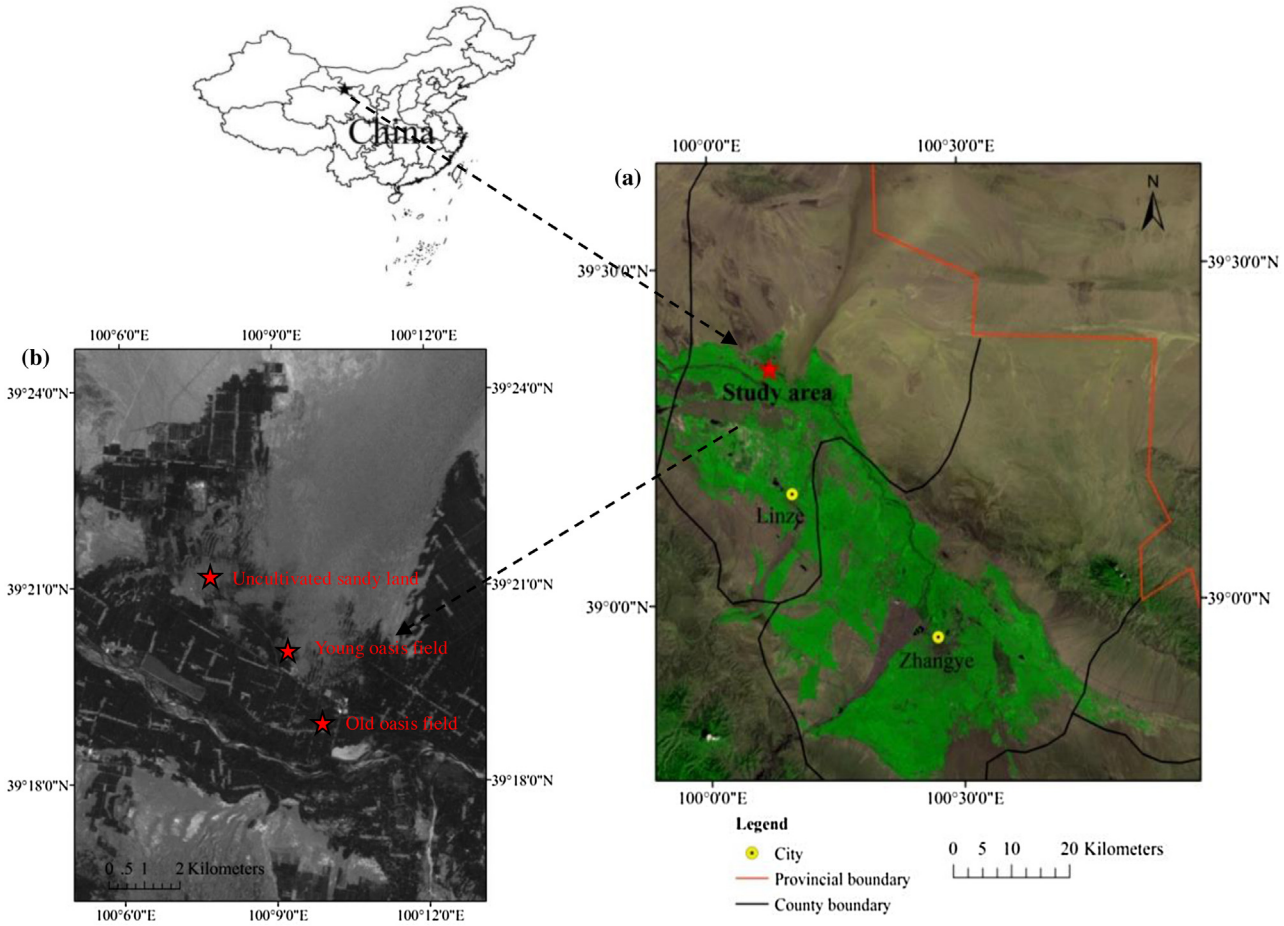

Fig. 1. Location of the study area (a) and soil sampling sites (b).

September 20th. The rate of fertilizer application was approximately 300–450 kg^{-1} N ha^{-1}, 90–150 kg^{-1} P_2O_5 ha^{-1}, and 60–90 kg^{-1} K_2O ha^{-1} each year. The annual farmyard manure application was about 3000–6000 kg ha^{-1}. Conventional tillage management has been commonly adopted. Typically, croplands are irrigated to store soil water in winter. The use of water resources for crop production is dependent on surface water (Heihe River) and groundwater. During the growing season, maize is irrigated 5–10 times (at planting time, sixth leaf stage, twelfth leaf stage, silking stage, milk stage, and physiological maturity) with more than 100 mm irrigation amount each time depending on different soil conditions (Su et al., 2010; Zhang et al., 2016). In the USL site, various plant species have been planted on sand dunes or in interdune lowlands to stabilize the dune. The predominant species include shrubs (*Caragana korshinskii*, *Haloxylon ammodendron*, *Hedysarum scoparium*) and annual sand-fixing desert plants (*Bassia All.*, *Eragrostis pilosa,* etc.). The planting of these drought-tolerant desert shrub species about 30–40 years ago was done to protect against sandstorms and to maintain a more stable environment in the desert-oasis region.

Soil profiles of the OOF, YOF, and USL sites are shown in Fig. 2. There are obvious soil horizons (plow layer, plow pan, and initial sandy layer) at the OOF and YOF sites, while the soil profile is uniform at the USL site. For each site, three replicated soil samples were collected to analyze soil properties. In addition, soil samples were taken from the plow layer (0–15 cm), the plow pan (15–30 cm), and the initial sandy layer (30–50 cm) in each plot. Soils were air-dried at room temperature before sieving to 2 mm for analysis of soil particle distribution. Soil particle size distribution was determined using the pipette method (Gee and Bauder, 1986). Subsamples, for the determination of soil organic carbon and total nitrogen, were ground to pass through a 0.25-mm sieve. Soil organic carbon was then measured using the dichromate oxidation method, and total nitrogen using the Kjeldahl method (Bao, 2000). Another subsample was passed through an 8-mm sieve to quantify aggregates. Soil dry aggregate size distribution was determined using the dry sieving method (Institute of Soil Sciences, 1978) and expressed as the mean weight diameter of aggregates. Dry mean weight diameter (DMWD) was calculated as follows (Su et al., 2010):

$$DMWD = \sum_{i=1}^{6} x_i w_i \quad (1)$$

where w_i is the mass percentage of aggregates remaining on the ith sieve; and x_i is the average diameter of the two adjacent size classes.

Undisturbed soil cores (5 cm in diameter, 5 cm in height) with three replicates were collected from each soil layer and then oven-dried at 105 °C for 48 h to measure soil bulk density using the dry weight of each column (Zhen et al., 2015). Total porosity was calculated according to (Shao et al., 2006): total porosity = (1 − bulk density/particle density) × 100. Generally, particle density of most soils is 2.65 g cm^{-3} (Zhen et al., 2015) used in our calculations.

The structural stability index (SI) is one way to assess the risk of soils being structural degraded. The SI was calculated for each

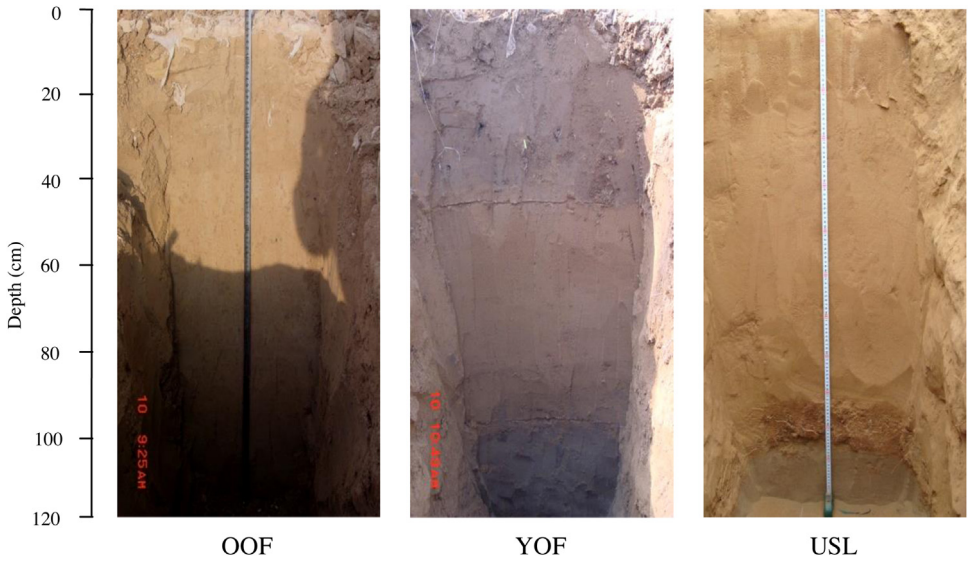

Fig. 2. Soil horizons from an old oasis field (OOF), young oasis field (YOF), and uncultivated sandy land (USL). There are obvious soil horizons at the OOF and YOF sites due to agricultural cultivation.

sample using the following formula (Asensio et al., 2013; Zhen et al., 2015):

$$SI = \frac{1.274 \times \ soil\ organic\ content}{silt\ +\ clay} \times 100 \quad (2)$$

where "(silt + clay)" (%) is the combined silt and clay content of the soil. SI > 9% indicates that the structure is stable; 7% < SI ≤ 9% indicates a low risk of structural degradation; 5% < SI ≤ 7% indicates a high risk of degradation; and SI ≤ 5% indicates structurally degraded soil (Asensio et al., 2013). In this study, soil properties and macropore characteristics determined in soil column samples were investigated after spring wheat harvest. These soil properties are summarized in Table 1.

To investigate the characteristics of 3-D soil macropore networks, four replicated intact soil columns (15 cm in diameter, 30 cm in height) were collected from 0 to 30 cm depths using PVC cylinders at each site. Only three replicates were collected at the USL site owing to one broken soil structure. Soil columns were sealed with plastic film and transported carefully to avoid any compaction and evaporation.

2.3. Quantification of soil macropores using CT scanning

Soil columns were scanned with a helical medical computed tomography (CT) (Optima CT520, GE, USA) with an excitation voltage of 100 kV at 100 mA in the Linze County People Hospital. Scan resolution was 0.469 mm horizontally and 0.600 mm vertically. Each column was scanned vertically and generated about 500 images of 512 pixels × 512 pixels. To remove edge effects, 25 images were discarded from the top of the column and 30 images were deleted from the bottom, with a resulting 445 images being analyzed for macropore structure. A sub-volume of 10.08 cm × 10.08 cm × 26.70 cm representing the inscribed cuboid of each column was extracted for soil macropore analysis. The

Table 1
Soil properties in an old oasis field (OOF), young oasis field (YOF), and uncultivated sandy land (USL), where averages are based on three replicates.

Sites	Depth (cm)	Particle size distribution (%)			Bulk density ($g\,cm^{-3}$)	Total porosity ($cm^3\,cm^{-3}$)	Soil organic carbon ($g\,kg^{-1}$)	Total nitrogen ($g\,kg^{-1}$)		
		Sand (0.05–2.00 mm)	Silt (0.002–0.05 mm)	Clay (<0.002 mm)					DMWD (mm)	SI (%)
Old oasis field (OOF)	0–15	61.04 ± 0.31	23.09 ± 0.12	15.87 ± 0.19	1.43 ± 0.02	0.46	11.55 ± 0.27	0.92 ± 0.04	3.75 ± 0.16	3.78 ± 0.12
	15–30	61.10 ± 0.81	23.10 ± 0.31	15.80 ± 0.64	1.46 ± 0.02	0.45	10.69 ± 0.03	0.82 ± 0.02	4.64 ± 0.32	3.51 ± 0.08
	30–50	60.59 ± 1.17	23.57 ± 0.82	15.84 ± 0.49	1.49 ± 0.03	0.44	10.04 ± 0.26	0.81 ± 0.03	/	/
Young oasis field (YOF)	0–15	71.07 ± 0.69	15.86 ± 0.54	13.07 ± 0.37	1.51 ± 0.01	0.43	7.57 ± 0.62	0.58 ± 0.01	3.32 ± 0.60	3.34 ± 0.28
	15–30	72.52 ± 0.97	15.41 ± 1.23	12.07 ± 0.26	1.56 ± 0.03	0.41	5.97 ± 0.48	0.52 ± 0.07	2.93 ± 0.63	2.77 ± 0.19
	30–50	82.93 ± 0.63	7.24 ± 0.80	9.83 ± 0.28	1.51 ± 0.02	0.43	4.07 ± 0.12	0.39 ± 0.03	/	/
Uncultivated sandy land (USL)	0–15	90.75 ± 0.45	2.97 ± 0.06	6.28 ± 0.45	1.58 ± 0.01	0.40	1.49 ± 0.15	0.10 ± 0.02	0.15 ± 0.00	2.08 ± 0.30
	15–30	91.18 ± 0.26	2.34 ± 0.06	6.48 ± 0.33	1.59 ± 0.05	0.40	1.58 ± 0.13	0.16 ± 0.02	0.16 ± 0.01	2.27 ± 0.12
	30–50	90.68 ± 0.34	2.60 ± 0.20	6.72 ± 0.20	1.54 ± 0.00	0.42	1.37 ± 0.09	0.11 ± 0.02	/	/

DMWD: dry mean weight diameter of aggregates, SI: structural stability index, Values represent means followed by the standard error.

scanned images were carefully examined to identify any soil columns that might have obvious sampling disturbance. Unnatural macropore morphology occurred in the bottom of the third OOF soil core column with high coarse fragments. Thus, a sub-volume of 10.08 cm × 10.08 cm × 24.12 cm representing the inscribed cuboid of the column was extracted for final analysis.

A global thresholding method was used for image binarization, with the threshold values carefully chosen based on visual observation using ImageJ 1.50e (Wayne Rasband, National Institues of Health, USA). Due to resolution limits, only pores with a diameter larger than 0.469 mm were recognized as macropores in this study. Since soil water content and other physical properties varied among the soil columns, different threshold values were obtained for each column (Table 2). The ImageJ plug-in 3D Viewer was used to visualize soil macropore networks. The ImageJ plug-in Measure Stack was used to measure macropore area density (the ratio of macropore area to the total studied image area), as it varies with soil depth for each soil column. Macroporosity, macropore length density, mean macropore length, and connectivity density were calculated using the BoneJ 1.3.11 plug-in in ImageJ (Doube et al., 2010). The connectivity density described the Euler characteristic of an image, which can be interpreted as trabecular number per volume (Doube et al., 2010). The total surface area of all macropores, macropore number, and mean macropore volume were obtained using the plug-in 3D Object Counter (Bolte and Cordelieres, 2006). Tortuosity was defined as the ratio of the total actual macropore length to the total straight-line distance (Luo et al., 2010a). Typically, equivalent hydraulic radius is used to characterize macropore size by assuming that the macropore is cylindrical (Hillel, 1998). The equivalent hydraulic radius was analyzed in order to investigate macropore properties in the entire soil column by skeletonizing 3-D macropores, which was calculated by the total volume and total length of the macropore (Luo et al., 2010a).

2.4. Statistical analysis

All data were expressed as means ± standard errors (SE) of the mean. Using the General Linear Model (GLM) procedure in SPSS, one-way analysis of variance (ANOVA) was used to examine the effect of cultivation period on soil properties and macropore characteristics. Tukey's post hoc test ($p < 0.05$) was applied to compare soil properties and macropore characteristics among study sites. Correlation coefficients were also calculated between soil properties and macropore variables. Statistical analysis was performed using the software program SPSS, ver. 17.0 (SPSS Inc., Chicago, IL, USA).

Table 2
Estimated lower and upper threshold levels to segregate CT image stacks of all soil columns from an old oasis field (OOF, 4 replicates), young oasis field (YOF, 4 replicates), and uncultivated sandy land (USL, 3 replicates).

Soil columns	Lower threshold level	Upper threshold level
OOF-1	0	130
OOF-2	0	110
OOF-3	0	120
OOF-4	0	115
YOF-1	0	95
YOF-2	0	105
YOF-3	0	95
YOF-4	0	100
USL-1	0	130
USL-2	0	125
USL-3	0	120
Mean	0	113

3. Results

3.1. Soil properties

Across the study sites, there was significant variation in particle size distribution of the soil profile, especially in the silt fraction (Table 1). The USL site with the deposition of aeolian sand was generally 90% sand (0.05–2.00 mm) and the soil was therefore classified as sandy soil (USDA classification system). Silt and clay contents at the YOF and OOF sites were higher than at USL and the soils were classified as sandy loam soil (USDA classification system). Total porosity increased from 40.67% at USL to 45% at OOF.

Analysis of variance of soil properties in the 0–30 cm soil profile among the three sites (OOF, YOF, and USL) revealed key differences among sites (Fig. 3). As cultivation time increased, silt and clay content increased, from 9.04% at USL to 38.93% at OOF. Soil organic carbon also increased, from 1.53 g kg^{-1} at USL to 11.12 g kg^{-1} at OOF, as did total nitrogen, from 0.13 g kg^{-1} at USL to 0.87 g kg^{-1} at OOF. One-way ANOVA found differences in silt and clay content, soil organic carbon, and total nitrogen across sites (Fig. 3a–c). The C/N ratio increased slightly after reclamation, but did not differ significantly among sites ($p > 0.05$) (Fig. 3d). Soil bulk density at OOF was 8.81% lower than at USL (Fig. 3e). The DMWD at USL, YOF, and OOF was 0.16 mm, 3.12 mm, and 4.19 mm, respectively. Dry soil aggregates differed significantly among sites (Fig. 3f). The structural stability index at the OOF site was 44.71% greater than at the USL site. In addition, the structural stability index also differed between YOF and USL (Fig. 3g). However, at all three sites the structural stability index measured less than 5%, indicating that all soils were structurally degraded. In conclusion, soil physico-chemical properties in irrigated croplands were more favorable for agriculture in comparison with uncultivated sandy land.

3.2. Soil macropore characteristics

Three-dimensional visualizations of soil macropore networks at the OOF, YOF, and USL sites are shown in Fig. 4. Cracks and other macropore characteristics were distinctly different comparing the soil columns from the three sites. Pores in the soil at OOF were more evenly distributed and more abundant than those at YOF, while YOF had more abundant pores again than USL. Relatively large and continuous macropores were distributed at OOF, and there were continuously tubular macropores in the third and fourth OOF soil columns. At YOF, more randomly and less continuously distributed macropores were likely cracks and inter-aggregated macropores. Few macropores were randomly scattered at USL. In irrigated croplands, cracks and macropores were mainly clustered in the upper part of the soil columns (0–200 mm), with macropore density decreasing with soil depth; few macropores were distributed at the bottom of the soil columns (plow pan). Soils developed more macropores as cultivation time increased.

Macropore characteristics of all soil columns as determined from CT images are shown in Table 3 for the three study sites. Macroporosity in soils at OOF were highest, 1.70%. With land reclamation and subsequent agricultural use, macroporosity and the total surface area increased such that these variables were greatest at OOF, followed by YOF, and the USL. Macroporosity at OOF was 18.89 times greater than at USL, while the total surface area at OOF was 11.25 times greater than at USL; both variables differed significantly among sites. Mean macropore volume was 20.71, 16.73, and 5.48 cm^3 at OOF, YOF, and USL sites, respectively; the difference between OOF and USL was significant. Mean macropore volume, macropore length density, and mean macropore length differed between OOF and USL. However, hydraulic radius, tortuosity, and connectivity density did not differ among

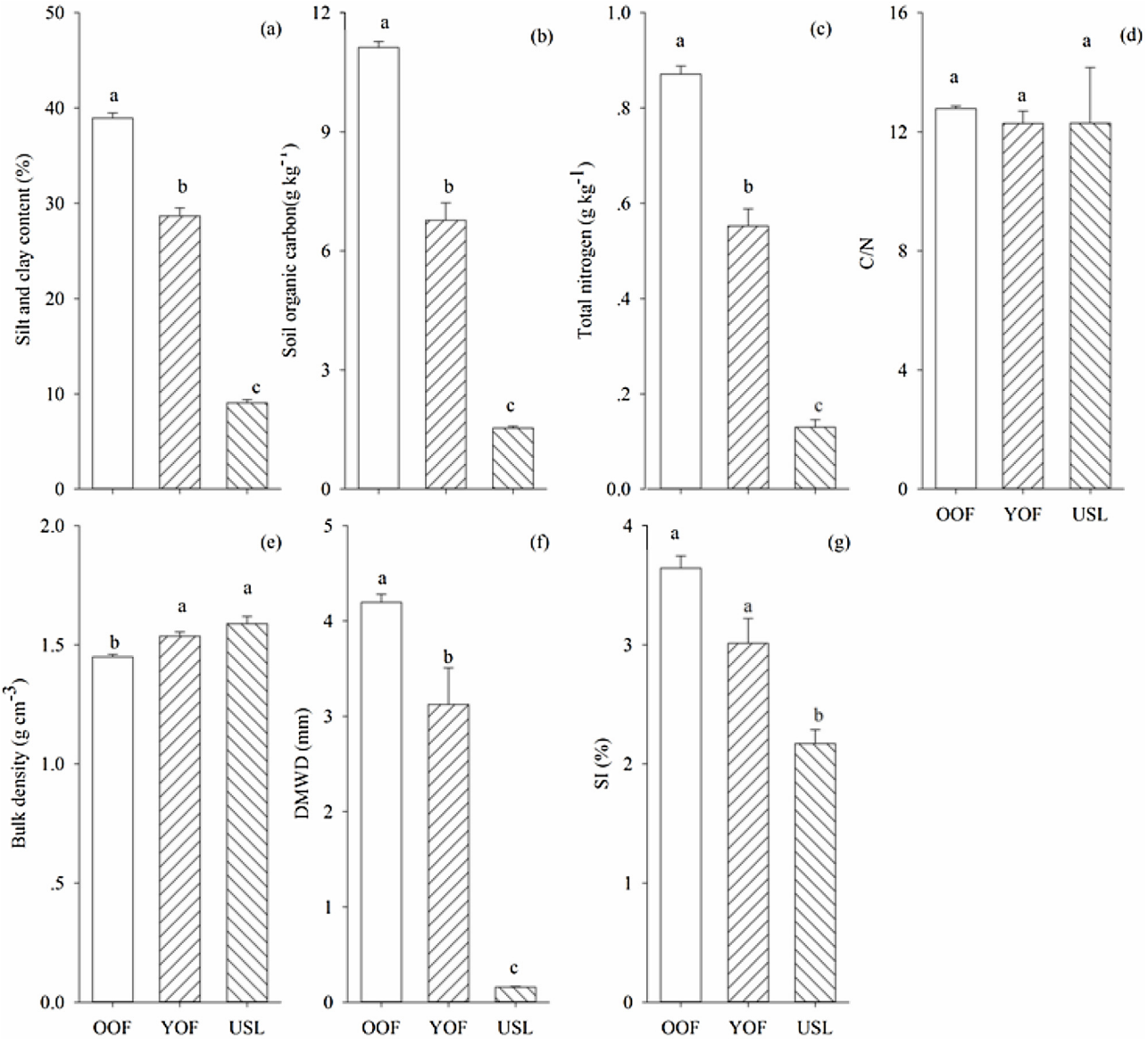

Fig. 3. Analysis of variance of silt and clay content (a), soil organic carbon (b), total nitrogen (c), C/N (d), bulk density (e), DMWD (f), and SI (g) in the 0–30 cm soil profile of an old oasis field (OOF), young oasis field (YOF), and uncultivated sandy land (USL).

the three sites ($p > 0.05$). Soils at OOF and YOF had greater macroporosity than soils at USL, and macroporosity increased as cultivation time increased.

Fig. 5 shows macropore area density distribution along the soil column for the three study sites. Macropore area density varied significantly among sample sites, with an order of OOF > YOF > USL. At OOF, macropore area density was greatest in surface soils, and generally decreased along soil depth. The first and fourth OOF columns had the highest macropore area density at about 80 mm and 130 mm of soil depth, respectively, indicating the existence of large soil cracks. At YOF, macropore area density was evenly distributed in the plow layer. There was also the higest macropore area density in the second and fourth YOF columns. In contrast, at USL, macropore area density was consistently very low (at less than 2%) along soil depth, indicating that few macropores were present. In summary, macropores were mainly distributed in the 0–200 mm soil layer at YOF and OOF, while only small and discontinuous macropores were found at USL.

The volume percentage (certain volume of macropore range to total soil volume) was calculated. Fig. 6 shows macropore volume distribution in the soil columns for the three study sites. Macropore volume distribution varied significantly among sites. At OOF, macropore volume distributions were similar for volumes less than 10 mm^3, but variation increased with macropore volume. For soils at YOF and USL, similar macropore volume distributions were observed for volumes less than 100 mm^3. The total volumes of macropores at OOF, YOF, and USL were less than 100,000 mm^3, 10,000 mm^3, and 1000 mm^3, respectively.

3.3. Relationships between soil macropore characteristics and physical properties

A correlation analysis, using data from all study sites, of macropore characteristics and soil property variables among the three sites is shown in Table 4. Significant positive correlations were found for silt and clay content, soil organic carbon, DMWD, and SI ($p < 0.05$); while significant negative correlations existed between bulk density and silt and clay content, soil organic carbon, DMWD, and SI ($p < 0.01$). In addition, there were significant positive correlations between macroporosity and total surface

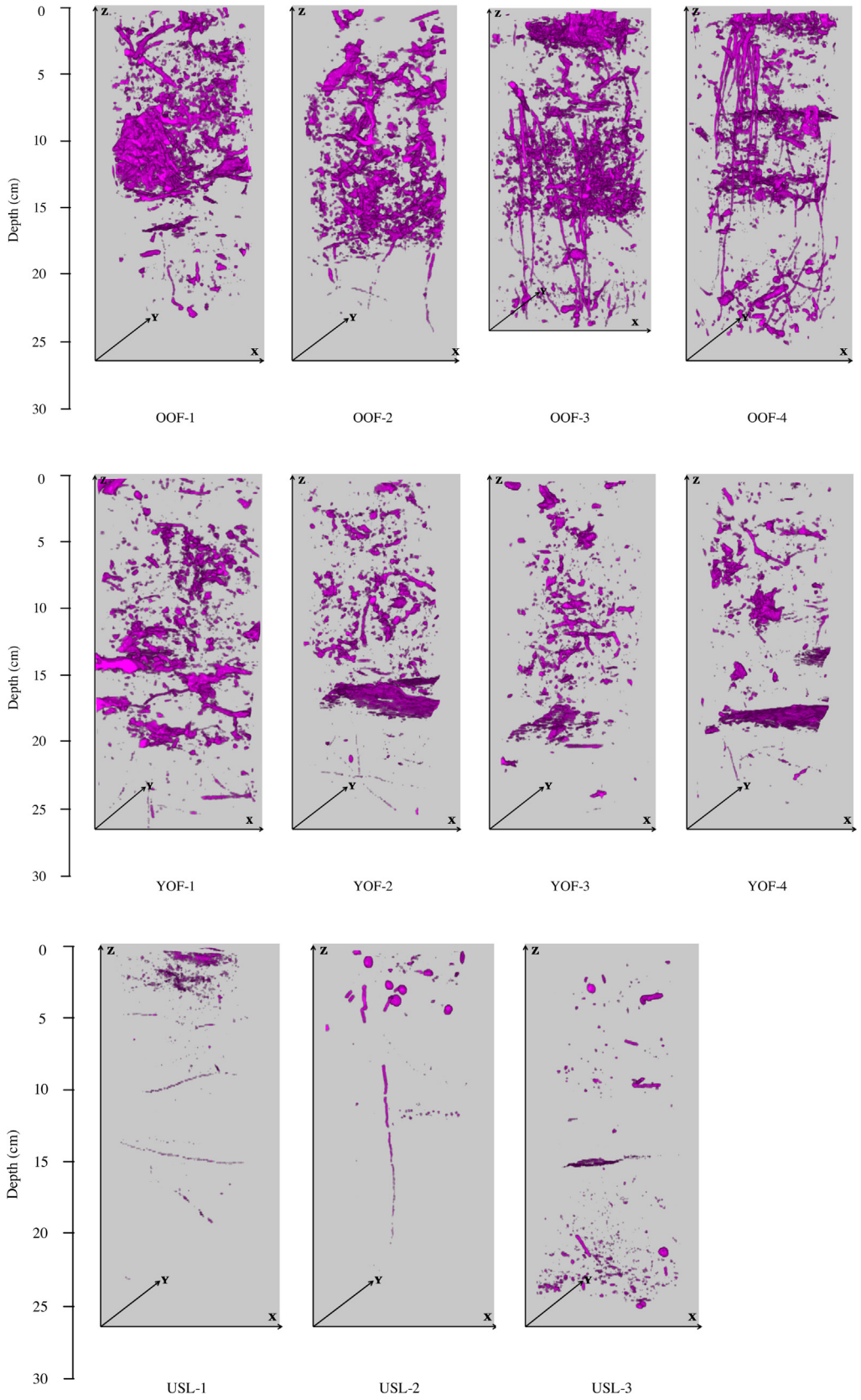

Fig. 4. Three-dimensional visualization of soil macropore networks in an old oasis field (OOF, 4 replicates), young oasis field (YOF, 4 replicates), and uncultivated sandy land (USL, 3 replicates). The scale of the OOF-3 soil core column is 10.08 cm × 10.08 cm × 24.12 cm, the rest of other soil core columns is 10.08 cm × 10.08 cm × 26.70 cm.

Table 3
Macropore characteristics of all soil columns determined from CT images in an old oasis field (OOF, 4 replicates), young oasis field (YOF, 4 replicates), and uncultivated sandy land (USL, 3 replicates).

Soil columns	Macroporosity (%)	SA ($cm^2\ cm^{-3}$)	MN	MV (mm^3)	MLD ($cm\ cm^{-3}$)	ML (cm)	HR (cm)	Tortuosity	CD (number cm^{-3})
OOF-1	2.06	0.45	2018	27.64	0.49	0.66	0.12	1.28	0.11
OOF-2	1.40	0.35	1528	24.89	0.36	0.64	0.11	1.29	0.01
OOF-3	2.00	0.60	3949	12.41	0.72	0.45	0.09	1.29	0.10
OOF-4	1.36	0.40	2052	17.91	0.47	0.62	0.10	1.24	0.04
Mean ± standard error	1.70 ± 0.19 a	0.45 ± 0.05 a	2387 ± 534 a	20.71 ± 3.44 a	0.51 ± 0.08 a	0.59 ± 0.05 a	0.10 ± 0.01 a	1.28 ± 0.01 a	0.07 ± 0.02 a
YOF-1	0.80	0.23	1902	11.46	0.25	0.35	0.10	1.29	0.01
YOF-2	0.70	0.21	1479	12.87	0.22	0.40	0.10	1.26	0.03
YOF-3	0.65	0.17	1028	17.03	0.17	0.44	0.11	1.27	0.02
YOF-4	0.78	0.18	831	25.54	0.19	0.63	0.11	1.25	0.03
Mean ± standard error	0.73 ± 0.04 b	0.20 ± 0.01 b	1310 ± 239 ab	16.73 ± 3.17 ab	0.21 ± 0.02 b	0.46 ± 0.06 a	0.11 ± 0.00 a	1.27 ± 0.01 a	0.02 ± 0.00 a
USL-1	0.06	0.04	840	2.05	0.07	0.22	0.05	1.27	0.01
USL-2	0.08	0.02	197	10.97	0.01	0.18	0.14	1.22	0.00
USL-3	0.13	0.05	1009	3.42	0.06	0.16	0.08	1.21	0.02
Mean ± standard error	0.09 ± 0.02 c	0.04 ± 0.01 c	682 ± 247 b	5.48 ± 2.77 b	0.05 ± 0.02 b	0.18 ± 0.02 b	0.09 ± 0.03 a	1.23 ± 0.02 a	0.01 ± 0.01 a

SA: total surface area of all macropores, MN: macropore number, MV: mean macropore volume, MLD: macropore length density, ML: mean macropore length, HR: hydraulic radius, CD: connectivity density.

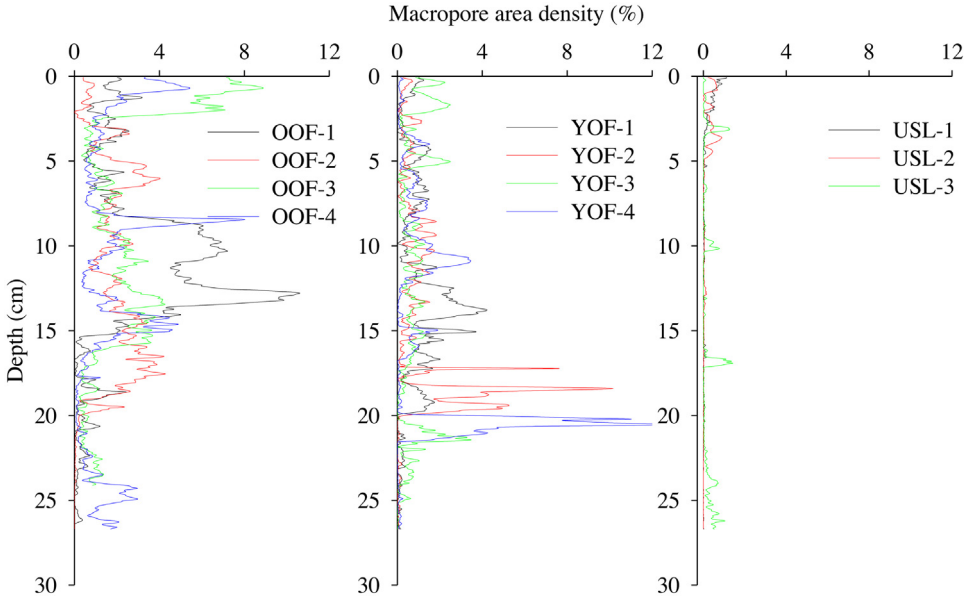

Fig. 5. Distribution of macropore area density along the soil core column depth from an old oasis field (OOF, 4 replicates), young oasis field (YOF, 4 replicates), and uncultivated sandy land (USL, 3 replicates).

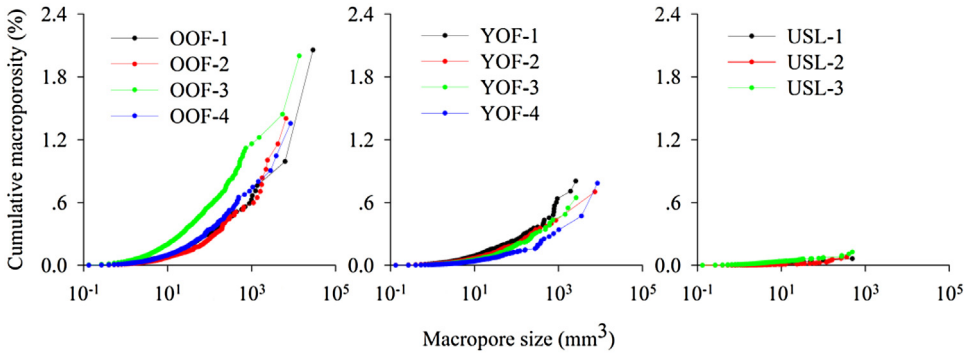

Fig. 6. Cumulative macropore volume distributions in soil core columns from an old oasis field (OOF, 4 replicates), young oasis field (YOF, 4 replicates), and uncultivated sandy land (USL, 3 replicates).

Table 4
Correlation analysis between soil properties and macropore features among the three sites.

Properties	Silt and clay content	Soil organic carbon	Bulk density	DMWD	SI	Macroporosity	SA	MN	MV	MLD	HR	Tortuosity	CD
Silt and clay content	1.000												
Soil organic carbon	0.818[b]	1.000											
Bulk density	−0.807[b]	−0.697[b]	1.000										
DMWD	0.600[b]	0.636[b]	−0.734[b]	1.000									
SI	0.564[a]	0.600[b]	−0.771[b]	0.673[b]	1.000								
Macroporosity	0.709[b]	0.818[b]	−0.624[b]	0.527[a]	0.709[b]	1.000							
SA	0.782[b]	0.891[b]	−0.697[b]	0.600[a]	0.636[b]	0.855[b]	1.000						
MN	0.673[b]	0.782[b]	−0.661[b]	0.564[a]	0.527[a]	0.673[b]	0.818[b]	1.000					
MV	0.491[a]	0.455[a]	−0.514[a]	0.309	0.564[a]	0.564[a]	0.418	0.236	1.000				
MLD	0.818[b]	0.855[b]	−0.734[b]	0.636[b]	0.673[b]	0.818[b]	0.964[b]	0.782[b]	0.382	1.000			
HR	0.096	0.058	−0.136	0.058	0.173	0.173	0.019	−0.135	0.559[a]	−0.019	1.000		
Tortuosity	0.359	0.472[a]	−0.419	0.548[a]	0.472[a]	0.359	0.434	0.434	0.170	0.472[a]	−0.020	1.000	
CD	0.610[a]	0.572[a]	−0.404	0.343	0.267	0.572[a]	0.610[a]	0.458	0.420	0.572[a]	−0.040	0.020	1.000

DMWD: dry mean weight diameter of aggregates, SI: structural stability index, SA: total surface area of all macropores, MN: macropore number, MV: mean macropore volume, MLD: macropore length density, HR: hydraulic radius, CD: connectivity density.
[a] Correlation significant at the 0.05 level (2-tailed).
[b] Correlation significant at the 0.01 level (2-tailed).

area, macropore number, mean macropore volume, and macropore length density ($p < 0.05$). Soil macroporosity was strongly positively correlated with both soil organic carbon and silt and clay content ($p < 0.01$), while it was negatively correlated with bulk density ($p < 0.01$). These results demonstrate that soil macropores may be strongly influenced by soil properties.

4. Discussion

4.1. Changes in soil physicochemical properties

Sustainable agricultural use of cultivated desert soils has become a concern in the Hexi Corridor of Northwestern China (Li et al., 2006). Knowledge of soil quality and how it changes with cultivation time are helpful in maintaining ecological stability in oases and in developing sustainable agriculture practices in arid regions (Huang et al., 2007; Li et al., 2009a, 2009b). After conversion of native desert soils to irrigated croplands, soil physicochemical properties can be altered due to land management practices such as conservation tillage, conversion of newly reclaimed farmlands to perennial grasslands, and crop and grass rotation (Su et al., 2010). In this study, soil physicochemical properties varied among soils from three contrasting sites. As cultivation time increased, silt and clay content and DMWD increased, whereas bulk density decreased. This is consistent with the results of Su et al. (2010), who reported significant changes in particle size distribution and aggregate size distribution and stability in the 0–20 cm soil depth only occurring in soils cultivated for more than 10 years, showing a consistently increasing pattern with increasing duration of cultivation. The favorable trend of soil properties for agriculture during the land conversion process can be attributed to agricultural management practices including irrigation, conservation tillage, and fertilization. Irrigation with silt-laden river water can result in an increase in the silt and clay content of soils. It is this increase in clay content as the binding agents, which can enhance the development of soil aggregates and decrease bulk density in desert soils.

Soil organic carbon and total nitrogen also increased as cultivation time increased in this study. Both Su et al. (2010) and Li et al. (2009a, 2009b) also found significant increase in soil organic C pool of desert soils after more than 10 years of cultivation in Northwest Chinese oases. This increase in both soil organic carbon and nutrient contents after conversion to agriculture was largely attributed to the inputs from manure and chemical fertilizers and from crop root decomposition after harvest. Fertilization improves crop yields, and this in turn increases root production; decomposed crop residuals may then increase soil organic carbon and nutrient input to soils. The farmyard manure application also increased soil organic carbon and changed soil aggregates. Moreover, in this study, a significant positive correlation was found between soil organic carbon and macroporosity in all the soil columns studied ($r^2 = 0.67$, $p < 0.01$ in Table 4). This is consistent with the results of Luo et al. (2010a). Organic matter enhances soil aeration promoting biological activity in soils of irrigated croplands; this effect could provide a positive feedback to further macropore development. In all the three study sites, the structural stability index was less than 5%, indicating structurally degraded soils. Soils derived from the deposition of aeolian sand presented a loose structure and a shortage of aggregates. Therefore, the conversion of virgin desert to sustainable agricultural land requires long time cultivation with improved land management practices. In conclusion, both the soil structure and physical properties in irrigated croplands presented a favorable trend comparable with soils from uncultivated sandy land.

4.2. Changes in soil macropore characteristics

As soil macropores control both soil water and solute transport, the visualization and quantification of macropore characteristics are essential for better understanding and prediction soil ecohydrological and geochemical functions (Jarvis, 2007; Li et al., 2009a, 2009b; Rab et al., 2014). Three-dimensional soil macropore networks as elucidated by CT were complicated and irregular (Fig. 4). Distinctly different types of macropores were observed among soil columns from the three study sites. Soils from OOF and YOF sites had greater macroporosity compared with USL soil, and macroporosity increased with cultivation time. Sparse and discontinuous macropores at the USL site were randomly distributed in soil columns. Biopores (earthworm burrows or root channels) are large tubular pores that are mostly vertically oriented (Katuwal et al., 2015). Smaller, more randomly and less continuously distributed macropores were likely inter-aggregate macropores, such as those formed by freezing and thawing or wetting and drying (Luo et al., 2010a). Long and continuously tubular macropores were likely biopores (OOF-3 and OOF-4 in Fig. 4). Crop roots were mostly concentrated in the soil plow layer (0–20 cm) (Fig. 2), as were their macropores (Fig. 4). Macropores

formed by root channels or decomposed crop residues accounted for some macropore networks at OOF and YOF sites. Therefore, the spatial distribution of soil macropores corresponded well with the position of roots in the soil profile (Fig. 2). Moreover, the greater, more randomly distributed macropores at OOF and YOF were likely inter-aggregate macropores, which probably formed by alternate wetting and drying processes (Luo et al., 2010a). In irrigated croplands, the spatial distribution of soil macropores also corresponded well with soil horizons in the soil profile (Fig. 2). Cracks and macropores were mainly concentrated in the 0–200 mm plow layer of the soil horizon. The large number of macropores found at OOF and YOF can likely be attributed to greater soil organic carbon, long time tillage-induced soil horizons, and alternate wetting and drying processes. The smaller and less continuously distributed macropores at USL may be associated with wind erosion and other physical processes; round and tubular paths in the soil were likely formed by soil fauna burrows. This study clearly demonstrates that cultivation has had positive effects on soil pore development.

5. Conclusions

This study was to quantify changes in soil properties and macropore features, using X-ray CT scanning, for three sites (OOF, YOF, and USL) in Northwest China. Cultivation played an important role in the changes of soil properties and macropore characteristics in this desert-oasis region. Silt and clay content, DMWD, soil organic carbon, and total nitrogen increased as cultivation time increased, whereas bulk density decreased. The structural stability index was less than 5% at all sites. Soils from the OOF and YOF sites had greater macroporosity compared with USL, and soils developed more, larger macropores as cultivation period increased. Soil macropores were observed mainly at 0–200 mm soil depth at YOF and OOF sites, while few macropores were found at USL and these were randomly distributed along soil depth. Soil pore structure and soil physicochemical properties in irrigated croplands were enhanced for agriculture following improved land management practices.

Acknowledgements

This work was supported by the National Natural Science Foundation of China (NO. 41401036, 41630861), the China Postdoctoral Science Foundation (NO. 2015T81070, 2014M560818). We are grateful to Dr. Jiliang Liu for providing the photos. We would also like to thank Emily Drummond at the University of British Columbia for her assistance with English language and grammatical editing of the manuscript. We also thank two anonymous reviewers and the editors for their constructive comments on this manuscript.

References

Abou Najm, M.R., Jabro, J.D., Iversen, W.M., Mohtar, R.H., Evans, R.G., 2010. New method for the characterization of three-dimensional preferential flow paths in the field. Water Resour. Res. 46, W02503.

Asensio, V., Vega, F.A., Andrade, M.L., Covelo, E.F., 2013. Tree vegetation and waste amendments to improve the physical condition of copper mine soils. Chemosphere 90 (2), 603–610.

Bandyopadhyay, K.K., Mohanty, M., Painuli, D.K., Misra, A.K., Hati, K.M., Mandal, K.G., Ghosh, P.K., Chaudhary, R.S., Acharya, C.L., 2003. Influence of tillage practices and nutrient management on crack parameters in a Vertisol of central India. Soil Tillage Res. 71 (2), 133–142.

Bao, S.D., 2000. Soil and Agricultural Chemistry Analysis. China Agriculture Press, Beijing (In Chinese).

Beven, K., Germann, P., 1982. Macropores and water flow in soils. Water Resour. Res. 18 (5), 1311–1325.

Bolte, S., Cordelieres, F.P., 2006. A guided tour into subcellular colocalization analysis in light microscopy. J. Microsc. 224 (3), 213–232.

Capowiez, Y., Pierret, A., Moran, C.J., 2003. Characterisation of the three–dimensional structure of earthworm burrow systems using image analysis and mathematical morphology. Biol. Fertil. Soils 38 (5), 301–310.

Doube, M., Kłosowski, M.M., Arganda-Carreras, I., Cordelières, F.P., Dougherty, R.P., Jackson, J.S., Schmid, B., Hutchinson, J.R., Shefelbine, S.J., 2010. BoneJ: free and extensible bone image analysis in Image. J. Bone 47, 1076–1079.

Gantzer, C.J., Anderson, S.H., 2002. Computed tomographic measurement of macroporosity in chisel–disk and no–tillage seedbeds. Soil Tillage Res. 64 (1), 101–111.

Gee, W.G., Bauder, J.W., 1986. Particle-size analysis. In: Klute, A. (Ed.), Methods of Soil Analysis. Part 1. Physical and Mineralogical Methods. American Society of Agronomy, Soil Science Society of America, Madison, WI, pp. 383Y412.

Grevers, M.C.J., Jong, E.D., St Arnaud, R.J., 1989. The characterization of soil macroporosity with CT scanning. Can. J. Soil Sci. 69 (3), 629–637.

Helliwell, J.R., Sturrock, C.J., Grayling, K.M., Tracy, S.R., Flavel, R.J., Young, I.M., Whalleyc, W.R., Mooneya, S.J., 2013. Applications of X-ray computed tomography for examining biophysical interactions and structural development in soil systems: a review. Eur. J. Soil Sci. 64 (3), 279–297.

Hillel, D., 1998. Environmental Soil Physics. Academic Press, San Diego, CA, pp. 120.

Hu, X., Li, Z.C., Li, X.Y., Liu, Y., 2015. Influence of shrub encroachment on CT-measured soil macropore characteristics in the Inner Mongolia grassland of northern China. Soil Tillage Res. 150, 1–9.

Hu, X., Li, Z.C., Li, X.Y., Liu, L.Y., 2016. Quantification of soil macropores under alpine vegetation using computed tomography in the Qinghai Lake Watershed, NE Qinghai–Tibet Plateau. Geoderma 264, 244–251.

Huang, J., Wang, R., Zhang, H., 2007. Analysis of patterns and ecological security trend of modern oasis landscapes in Xinjiang, China. Environ. Monit. Assess. 134 (1–3), 411–419.

Institute of Soil Sciences, Chinese Academy of Sciences, 1978. Physical and Chemical Analysis Methods of Soils. Shanghai Science Technology Press, Shanghai,C hina. [In Chinese].

Jarvis, N.J., Moeys, J., Koestel, J., Hollis, J.M., 2012. Preferential flow in a pedological perspective. In: Lin, H. (Ed.), Hydropedology: Synergistic Integration of Soil Science and Hydrology. Academic Press, Elsevier B.V., pp. 75–120.

Jarvis, N.J., 2007. A review of non-equilibrium water flow and solute transport in soil macropores: principles, controlling factors and consequences for water quality. Eur. J. Soil Sci. 58 (3), 523–546.

Jassogne, L., McNeill, A., Chittleborough, D., 2007. 3D-visualization and analysis of macro- and meso-porosity of the upper horizons of a sodic, texture-contrast soil. Eur. J. Soil Sci. 58 (3), 589–598.

Katuwal, S., Norgaard, T., Moldrup, P., Lamandé, M., Wildenschild, D., de Jonge, L.W., 2015. Linking air and water transport in intact soils to macropore characteristics inferred from X-ray computed tomography. Geoderma 237, 9–20.

Kumar, S., Anderson, S.H., Udawatta, R.P., 2010. Agroforestry and grass buffer influences on macropores measured by computed tomography under grazed pasture systems. Soil Sci. Soc. Am. J. 74 (1), 203–212.

Li, X.G., Li, F.M., Rengel, Z., Wang, Z.F., 2006. Cultivation effects on temporal changes of organic carbon and aggregate stability in desert soils of Hexi Corridor region in China. Soil Tillage Res. 91 (1), 22–29.

Li, X.G., Li, Y.K., Li, F.M., Ma, Q., Zhang, P.L., Yin, P., 2009a. Changes in soil organic carbon, nutrients and aggregation after conversion of native desert soil into irrigated arable land. Soil Tillage Res. 104 (2), 263–269.

Li, X.Y., Yang, Z.P., Li, Y.T., Lin, H., 2009b. Connecting ecohydrology and hydropedology in desert shrubs: stemflow as a source of preferential flow in soils. Hydrol. Earth Syst. Sci. 13 (7), 1133–1144.

Li, T.C., Shao, M.A., Jia, Y.H., 2016. Application of X-ray tomography to quantify macropore characteristics of loess soil under two perennial plants. Eur. J. Soil Sci. 67 (3), 266–275.

Lin, H.S., McInnes, K.J., Wilding, L.P., Hallmark, C.T., 1996. Effective porosity and flow rate with infiltration at low tensions into a well-structured subsoil. Trans. ASABE 39 (1), 131–135.

Lin, H., Bouma, J., Wilding, L.P., Richardson, J.L., Kutilek, M., Nielsen, D.R., 2005. Advances in hydropedology. Adv. Agron. 85, 1–89.

Luo, L., Lin, H., Li, S., 2010a. Quantification of 3–D soil macropore networks in different soil types and land uses using computed tomography. J. Hydrol. 393 (1), 53–64.

Luo, L., Lin, H., Schmidt, J., 2010b. Quantitative relationships between soil macropore characteristics and preferential flow and transport. Soil Sci. Soc. Am. J. 74 (6), 1929–1937.

Luxmoore, R.J., Jardine, P.M., Wilson, G.V., Jones, J.R., Zelazny, L.W., 1990. Physical and chemical controls of preferred path flow through a forested hillslope. Geoderma 46 (1), 139–154.

Mooney, S.J., Morris, C., 2008. A morphological approach to understanding preferential flow using image analysis with dye tracers and X-ray computed tomography. Catena 73 (2), 204–211.

Peng, X., Horn, R., Peth, S., Smucker, A., 2006. Quantification of soil shrinkage in 2D by digital image processing of soil surface. Soil Tillage Res. 91 (1), 173–180.

Rab, M.A., Haling, R.E., Aarons, S.R., Hannah, M., Young, I.M., Gibson, D., 2014. Evaluation of X-ray computed tomography for quantifying macroporosity of loamy pasture soils. Geoderma 213, 460–470.

Ringrose-Voase, A.J., Sanidad, W.B., 1996. A method for measuring the development of surface cracks in soils: application to crack development after lowland rice. Geoderma 71 (3), 245–261.

Shao, M.A., Wang, Q.J., Huang, M.B., 2006. Soil Physics. Higher Education Press, Beijing, China (In Chinese).

Su, Y.Z., Zhao, W.Z., Su, P.X., Zhang, Z.H., Wang, T., Ram, R., 2007. Ecological effects of desertification control and desertified land reclamation in an oasis-desert ecotone in an arid region: a case study in Hexi Corridor, northwest China. Ecol. Eng. 29 (2), 117–124.
Su, Y.Z., Yang, R., Liu, W.J., Wang, X.F., 2010. Evolution of soil structure and fertility after conversion of native sandy desert soil to irrigated cropland in arid region, China. Soil Sci. 175 (5), 246–254.
Turberg, P., Zeimetz, F., Grondin, Y., Elandoy, C., Buttler, A., 2014. Characterization of structural disturbances in peats by X-ray CT-based density determinations. Eur. J. Soil Sci. 65 (4), 613–624.
Udawatta, R.P., Anderson, S.H., Gantzer, C.J., Garrett, H.E., 2008. Influence of prairie restoration on CT-measured soil pore characteristics. J. Environ. Qual. 37 (1), 219–228.
Zhang, Y.Y., Zhao, W.Z., 2015. Effects of variability in land surface characteristicson the summer radiation budget across desert–oasis region in Northwestern China. Theor. Appl. Climatol. 119 (3–4), 771–780.
Zhang, Z.B., Peng, X., Zhou, H., Lin, H., Sun, H., 2015. Characterizing preferential flow in cracked paddy soils using computed tomography and breakthrough curve. Soil Tillage Res. 146, 53–65.
Zhang, Y.Y., Zhao, W.Z., He, J.H., Zhang, K., 2016. Energy exchange and evapotranspiration over irrigated seed maize agroecosystems in a desert-oasis region northwest China. Agric. For. Meteorol. 223, 48–59.
Zhang, F.R., 2001. Pedogeography. Agricultural Press, Beijing, China (In Chinese).
Zhao, H.L., Zhou, R.L., Zhang, T.H., Zhao, X.Y., 2006. Effects of desertification on soil and crop growth properties in Horqin sandy cropland of Inner Mongolia, north China. Soil Tillage Res. 87 (2), 175–185.
Zhen, Q., Ma, W., Li, M., He, H., Zhang, X., Wang, Y., 2015. Effects of vegetation and physicochemical properties on solute transport in reclaimed soil at an opencast coal mine site on the Loess Plateau, China. Catena 133, 403–411.